cosmetics

MDPI

Article

Safflower Seed Oil Ameliorates AFL-Induced Epidermal Lipid Loss Partially via the PPARγ Signaling Pathway

Jinjin Liu [1,†], Qian Wang [2,†], Jialin Zhong [1,†], Xiaoqing Wang [1], Haidong Jia [2], Yushu Wang [1], Yuanyuan Chen [2,*], Runshuang Lu [2,*] and Gang Ma [1,*]

[1] Key Laboratory for the Genetics of Developmental and Neuropsychiatric Disorders (Ministry of Education), Bio-X Institutes, Shanghai Jiao Tong University, Shanghai 200240, China; nebula0808@sjtu.edu.cn (J.L.)
[2] Shanghai Jahwa United Co., Ltd., Shanghai 200233, China
* Correspondence: chenyuanyuan1@jahwa.com.cn (Y.C.); lurunshuang@jahwa.com.cn (R.L.); magang@sjtu.edu.cn (G.M.); Tel.: +86-21-34207232 (G.M.)
† These authors contributed equally to this work.

Abstract

Objective: Ablative fractional laser (AFL) therapy impairs epidermal barrier integrity through the disruption of stratum corneum lipids and keratinocyte differentiation, resulting in increased transepidermal water loss (TEWL) and delayed functional recovery. This study aims to develop a more effective barrier repair strategy and evaluate the efficacy of topical safflower seed oil (SSO) in promoting post-AFL barrier restoration. **Methods**: An optimized murine AFL model (20 W, 0.5 ms pulse delay, and 0.7 mm spot spacing) was established to investigate skin repair mechanisms. SSO composition was characterized by gas chromatography–mass spectrometry (GC-MS). Epidermal repair was assessed using confocal laser scanning microscopy, while Oil Red O staining and immunofluorescence were employed to evaluate lipid formation and the expression of lipid synthesis-related genes, respectively. **Results**: GC-MS analysis identified SSO as a rich natural source of linoleic acid (69.1%) and oleic acid (18.7%). Over the 7-day period of AFL exposure alone, TEWL rose by 4–6 fold in mouse skin, accompanied by a near-complete loss of epidermal lipid synthesis. However, upon SSO administration, a marked reduction in TEWL was observed from day 1, and epidermal lipid synthesis recovered by day 7. Moreover, SSO treatment significantly upregulated epidermal PPARγ expression in AFL-injured skin. Pharmacological inhibition of PPARγ (T0070907) largely abrogated the lipid synthesis and barrier repair effects of SSO, while PPARα antagonism (GW6471) showed no obvious interference with SSO's therapeutic efficacy, suggesting a potential association between PPARγ signaling modulation and SSO-mediated skin barrier restoration. **Conclusions**: These findings suggest that SSO is a promising natural agent for post-AFL skin care, which improves AFL-impaired skin barrier function by remodeling lipid metabolism, at least in part through PPARγ signaling, and warrants further preclinical and clinical investigation.

Keywords: ablative fractional laser; safflower seed oil; PPARγ; lipid metabolism; skin

Check for updates

Academic Editor: Richard Daniellou

Received: 26 July 2026
Revised: 7 September 2026
Accepted: 8 September 2026
Published: 11 September 2026

Copyright: © 2026 by the authors. Licensee MDPI, Basel, Switzerland. This article is an open access article distributed under the terms and conditions of the Creative Commons Attribution (CC BY) license.

1. Introduction

As the body's outermost organ, the skin serves as a protective barrier against environmental insults while maintaining hydrohomeostasis and facilitating sensory transduction [1]. Its stratified architecture, comprising the epidermis, dermis and hypodermis, demonstrates compartmentalized biological specialization, with each layer executing distinct physiological functions [2]. The epidermis comprises four strata: the stratum basal

(K5/K14+ keratinocytes for renewal) [3], stratum spinosum (K1/K10+ filaments for mechanical strength) [4], stratum granulosum (lamellar body secretion of lipid precursors), and stratum corneum (SC). Central to these roles is the SC, the outermost epidermal layer, which forms a strong physicochemical barrier through its unique 'brick wall' structure [5]. In this model, corneocytes are embedded in a lipid matrix composed of ceramides, cholesterol, and free fatty acids in an optimal 1:1:1 molar ratio [6]. This organization minimizes TEWL via hydrophobic lipid lamellae while restricting xenobiotic penetration through densely packed corneocytes [7,8]. Keratinocyte differentiation drives barrier formation through sequential keratin expression, lamellar body-mediated lipid secretion, and covalent cross-linking of cornified envelope proteins [9]. Ablative fractional laser (AFL) therapies, particularly CO_2 lasers (10,600 nm), are extensively utilized in treating photodamage and scars by creating microthermal treatment zones (MTZs) that vaporize epidermal and superficial dermal tissues. While AFL effectively stimulates collagen remodeling and wrinkle reduction [10,11], the procedure concurrently compromises barrier function by ablating the SC and disrupting the intercellular lipid matrix, leading to increased TEWL, erythema, and persistent sensitivity [12–14]. Current post-procedural care protocols often fail to adequately address the acute lipid metabolic dysregulation induced by AFL. Impaired lipid synthesis (e.g., ceramide depletion) and impaired keratinocyte differentiation contribute to conditions such as xeroderma, atopic dermatitis, and psoriasis, where barrier dysfunction exacerbates inflammation and sensitivity to irritants [15,16].

Peroxisome proliferator-activated receptors (PPARs) α, β/δ, and γ are critical regulators of epidermal lipid metabolism and barrier repair. While PPARβ/δ are most abundantly expressed in human epidermis, PPARα and γ are expressed at lower levels, but all have a significant effect on barrier repair [17]. PPARα activation enhances cholesterol and ceramide synthesis in keratinocytes and restores lipid homeostasis in barrier-disrupted models [18]. PPARβ/δ promotes keratinocyte differentiation and lipid accumulation by upregulating key enzymes such as fatty acid synthase, triglyceride synthase, and the lipid transporter ATP-binding cassette subfamily A member 12 (ABCA12), which facilitates lipid delivery into lamellar bodies [19]. PPARγ synergistically modulates enzymatic activity critical for ceramide generation, including β-glucocerebrosidase (GBA) [20]. Natural plant-derived compounds target these PPAR pathways to repair barrier dysfunction. Linoleic acid, a major component of safflower seed oil (SSO), acts as a PPARα agonist, elevating ceramide synthesis [21]. Oat oil activates both PPARα and PPARβ/δ, increasing ceramide levels by 70% through the upregulation of sphingomyelin phosphodiesterase 3 (SMPD3) and ABCA12 [22,23]. Tiliroside [24], a polyphenol from strawberry seeds, enhances glucosylceramide synthase (GCS) and GBA activity via PPARα [25], boosting stratum corneum ceramide production. Cinnamate derivatives function as dual PPARα/γ agonists, improving lipid barrier function by regulating fatty acid synthase and cholesterol metabolism enzymes [26]. These botanicals employ distinct PPAR-mediated mechanisms, which modulate lipid synthesis enzymes [27] and transporters [28], to provide multidimensional strategies for barrier restoration [29].

SSO, a natural botanical extract enriched in linoleic acid, holds therapeutic potential for repairing AFL-induced skin barrier disruption, yet its efficacy and mechanism remain poorly understood. The primary objective of this study was to investigate whether SSO can reestablish barrier homeostasis in AFL-damaged skin and to determine whether this effect is mediated, at least in part, through PPARγ-associated lipid metabolic pathways. By examining the relationship between SSO, PPARγ, and epidermal lipid synthesis, we sought to provide a mechanistic basis for the potential use of SSO as an adjunctive strategy for acute barrier repair following AFL procedures.

2. Materials and Methods

2.1. Mice

Male C57BL/6 mice (7–8 weeks, 18–22 g) were purchased from Shanghai SLAC Laboratory Animal Co., Ltd. (Shanghai, China), and were maintained in specific pathogen-free (SPF) facilities. Standard housing conditions comprised: (1) group size $\leq$ 5 animals/cage, (2) autoclaved chow and filtered water available ad libitum, and (3) controlled 12 h light/dark cycles (22 $\pm$ 1 °C, 50 $\pm$ 10% humidity). Environmental enrichment and sterile bedding renewal were performed every 48 h.

2.2. Safflower Seed Oil (SSO)

SSO, a fixed oil, was provided by Northstar Lipids (Lincolnshire, UK) Ltd. Its source and preparation were described following a previous study on safflower seed oil obtained by cold pressing and solvent extraction [30], together with the supplier's specifications. Briefly, SSO is derived from the seeds of Carthamus tinctorius and appears as a transparent lipid ranging from pale yellow to golden, with an almost odorless characteristic. It is mainly composed of fatty acids. Crude SSO is initially obtained by cold-pressing the seeds at temperatures below 60 °C. Subsequently, hexane is used to recover 30–40% of the residual oil from the press cake, with the final hexane residue controlled at $\leq$1 ppm. The oil is further refined to remove free fatty acids, pigments, pesticides, and trace elements, resulting in a solvent-residue-free product that complies with EU standards for edible oils. According to the supplier's specifications, the oil is certified as 100% natural under ISO 16128 [31].

2.3. Gas Chromatography–Mass Spectrometry (GC-MS) Analysis

The compositional analysis of SSO was carried out by GC-MS based on the method reported by Bouallegue et al., with minor modifications [32]. Briefly, SSO was analyzed using a GC-MS system equipped with an Agilent 19091S-433 HP-5ms capillary column. The inlet temperature was set at 50 °C, with a split ratio of 35:1 and a carrier gas flow rate of 1.2 mL/min. The column oven temperature was programmed to increase from 50 °C to 320 °C. Solvent blank runs were conducted prior to sample analysis to exclude potential contamination. After the baseline was stabilized, the sample was injected, and the total ion chromatogram (TIC) and corresponding mass spectra were recorded. The chemical constituents of SSO were qualitatively identified by spectral library matching based on retention time and characteristic ions. All analyses were performed by Shanghai Weipu Testing Technology Co., Ltd. (Shanghai, China).

2.4. AFL-Induced Damage of Murine Skin and SSO Treatment

For AFL mice: Mice were randomly allocated to six groups of five animals each. Before laser treatment, the dorsal hair was shaved using an electric clipper, followed by depilation with a depilatory cream. The exposed dorsal skin was then subjected to AFL treatment to simulate the clinical therapeutic process. Two AFL parameter settings were evaluated: Protocol A, 20 W power, 0.5 ms pulse duration, 0.7 mm spot spacing, and a fractional array area of 15 $\times$ 15 mm; and Protocol B, 30 W power, 10 ms pulse duration, 0.6 mm spot spacing, and a fractional array area of 15 $\times$ 15 mm. The optimal AFL model was selected based on histological evaluation. AFL treatment was performed using an LJL35-CS CO_2 fractional laser system (Shanghai Laser Institute, Shanghai, China).

For SSO treatment: Mice were randomly divided into three groups (5 mice per group): control group (shaved back, no AFL treatment); AFL group, AFL treatment alone; AFL-SSO group, AFL treatment followed by daily topical application of SSO (100 µL per application, provided by Shanghai Jahwa United Co., Ltd., Shanghai, China) twice daily for 7 days [33].

TEWL was assessed using a GPSkin Barrier® device (GPOWER, Seoul, Republic of Korea) at 12 h post-AFL and on days 1, 3, 5, and 7 (P1, P3, P5, and P7). Before each TEWL measurement, wound healing progress was documented photographically. Three random sites on the dorsal skin of each mouse were analyzed for statistical evaluation.

2.5. Peroxisome Proliferator-Activated Receptor (PPAR) Antagonist Intervention

For intraperitoneal (i.p.) administration, mice were randomly divided into three groups (5 mice per group): GW6471 (PPARα antagonist, 20 mg/kg in 10% DMSO, TargetMol, Shanghai, China) was injected every other day, T0070907 (PPARγ antagonist, 1 mg/kg in 10% DMSO, TargetMol, Shanghai, China) was injected daily for 7 days, and 10% DMSO was injected as vehicle control. For topical application, mice also were randomly divided into three groups (5 mice per group): GW6471 (20 mg/kg) was applied every other day, T0070907 (1 mg/kg) was applied daily for 7 days, and 10% DMSO was applied as vehicle control.

2.6. Hematoxylin and Eosin (H&E) Staining

Dorsal skin tissues were fixed in 4% paraformaldehyde (PFA) for 24–48 h, followed by sequential dehydration through graded ethanol series (70% to 100%), clearing in xylene, and embedding in paraffin wax (70 °C). Tissue sections of 4–6 μm thickness were prepared using a rotary microtome and dried at 50 °C. H&E staining (C0105S, Beyotime, Shanghai, China) was performed as follows: dewaxing in xylene, rehydration through descending ethanol gradients, nuclear staining with Harris hematoxylin (5 min), bluing in running water (10 min), cytoplasmic counterstaining with 0.5% eosin (1 min), dehydration in ascending ethanol series, and final mounting with neutral resin. Epidermal thickness was quantified using ImageJ software 1.54p.

2.7. Oil Red O Staining

Stock solution (0.5 g Oil Red O in 100 mL 99% isopropanol, 4 °C dark storage $\geq$ 24 h) was prepared; working solution: stock solution: ddH_2O (3:2); the solution was filtered (0.2 μm) or centrifuged (8000 rpm × 2 min). Then, 60% isopropanol was pre-cooled at 4 °C. Frozen sections were rinsed 3 times in Phosphate-Buffered Saline (PBS) (5 min each), fixed with 4% PFA (30 min, fume hood), and washed in PBS for 2 times. Then, they were pre-treated with 60% isopropanol (5 min), stained in working solution (15–30 min, dark), de-stained in 60% isopropanol (1 min), and rinsed with H_2O (5 min). Counterstaining was performed with filtered hematoxylin (0.22 μm, 5 min), followed by rinsing, differentiation in acidic ethanol (10 s), and bluing in H_2O (15 min), before air-drying, mounting with pre-warmed glycerol gelatin, and imaging immediately; slides were then stored in the dark $\leq$ 24 h.

2.8. Immunofluorescence Staining

Paraffin sections underwent dual xylene dewaxing (10 min × 2), graded ethanol rehydration (100% → 70%, 5 min/step), rinsing with ddH_2O, and 99 °C heat-induced antigen retrieval (20 min). After cooling, sections were washed with Phosphate-Buffered Saline with Tween 20 (PBST) (5 min × 3). Frozen sections retrieved from −80 °C were equilibrated at 42 °C and gently rinsed with PBS (10 min × 3). Immunofluorescence staining procedures included the following: sections were blocked in PBS with 10% Fetal Bovine Serum (FBS) for 1 h at room temperature (RT), followed by primary antibody incubation (4 °C/16–18 h) and Alexa Fluor-conjugated secondary antibody labeling (1:800, light-protected/2 h/RT). After PBS washes, slides were mounted with DAPI-containing ProLong™ Gold Antifade reagent, sealed, and imaged using a Leica SP8 (Leica Microsystems, Wetzlar, Germany) confocal system (4 °C storage).

The following antibodies were used for immunostaining: Chicken anti-K14 (Biolegend, 906004), Rabbit anti-PPARα (AiFang, AF3096), Mouse anti-PPARβ (HUABIO, ER1902-24), Rabbit anti-PPARγ (AiFang, AFW0270), Donkey anti-Rabbit IgG (H + L), Alexa Fluor™ Plus 594 (Thermo Fisher Scientific, Waltham, MA, USA, R37119), Donkey anti-Mouse IgG (H + L), Alexa Fluor™ Plus 594 (Thermo Fisher Scientific, R37115), and Donkey anti-Chicken IgY (H + L), Alexa Fluor™ 488 (Thermo Fisher Scientific, A78948).

2.9. RNA Isolation and Quantitative Reverse Transcription PCR (qRT-PCR)

Total RNA was isolated from murine dorsal skin and cultured cell lines utilizing TRIzol® Reagent (Vazyme Biotech, Nanjing, China, Cat# R401-01) in accordance with the manufacturer's protocol under RNase-free conditions. Subsequently, RNA (up to 1 μg) was used to synthesize cDNA using the HiScript III 1st Strand cDNA Synthesis System (Vazyme, Cat# R312-01). qRT-PCR was conducted employing SYBR Green Master Mix (Vazyme, Cat# Q311-02) with thermocycling parameters optimized for target amplification. The 18s ribosomal RNA gene was selected as an endogenous reference for data normalization across experimental samples. Relative gene expression was calculated using the $2^{-\Delta\Delta Ct}$ method. Primer sequences, the reaction system and amplification conditions are detailed in Supplemental Tables S1, S2 and S3, respectively.

2.10. Statistical Analysis

All experiments were performed with at least five biological replicates. When applicable, data were expressed as mean ± SEM. Statistical analyses were conducted using GraphPad Prism version 10. For comparisons between two groups, Student's two-tailed t test was used. For multiple group comparisons, one-way or two-way analysis of variance (ANOVA) was performed, followed by Tukey's multiple comparisons test or the Brown–Forsythe test as appropriate. Statistical significance was defined as * $p < 0.05$, ** $p < 0.01$, *** $p < 0.001$, and **** $p < 0.0001$; 'ns' indicates no statistically significant results.

3. Results

3.1. Component Characterization of SSO

SSO, a plant oil extracted from *Carthamus tinctorius* L. seeds, was characterized using GC-MS, revealing 42 characteristic compounds. The chemical composition predominantly comprised lipids, aliphatic aldehydes, and oxygenated terpenoids.

The lipid profile was dominated by 2-linoleoylglycerol (57.10%), followed by trilinolein (19.54%) and ethyl linoleate (5.33%), with additional structural diversity from free fatty acids (linoleic acid, 5.28%) and glycidyl palmitate (4.11%). Aldehydes included trans-2,4-decadienal (0.99%) and 2,4-decadienal (0.70%), while betulin (1.69%) represented the sole terpenoid. Trace components such as 1,2-dipalmitin (0.56%) and glycerol monooleate (0.37%) further enriched the lipid complexity, establishing SSO as a glycerol ester-rich system with structural heterogeneity and functional potential (Figure 1; Supplemental Table S4).

Fatty acid profiling revealed a predominance of unsaturated species (Supplemental Table S5), with linoleic acid (C18:2n6c, 69.1%) and oleic acid (C18:1n9c, 18.7%) constituting 88.7% of total fatty acids, alongside minor α-linolenic acid (Table S4). Polyunsaturated fatty acids (PUFAs) are critical for skin barrier integrity; clinical studies demonstrate $n-3$ PUFAs alleviate psoriasis by suppressing inflammatory cytokines [34], while in vitro models show α-linolenic and linoleic acids enhance barrier function through incorporation into phospholipids/triglycerides and regulation of bioactive lipids [35].

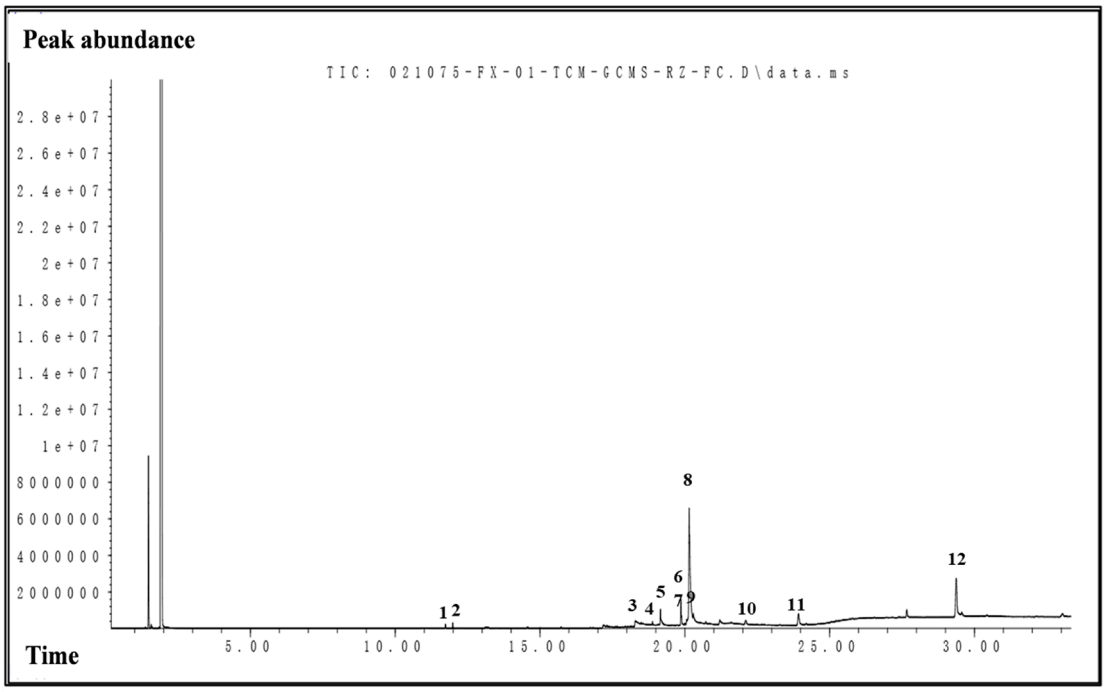


Figure 1. GC-MS total ion chromatogram of SSO. The chromatogram shows the peak abundance of components separated from SSO over time, providing a preliminary profile of its chemical composition. Peak 1: 2,4-Decadienal; Peak 2: trans-2,4-Decadienal; Peak 3: Linoleic acid; Peak 4: 1,2-Dipalmitoylglycerol; Peak 5: Glycidyl palmitate; Peak 6: 1-Monolinolein; Peak 7: Glyceryl monooleate; Peak 8: 2-Linoleoyl-rac-glycerol; Peak 9: Stearic acid glycidyl ester; Peak 10: Betulin; Peak 11: Ethyl linoleate; Peak 12: Trilinolein.

3.2. Establishment of an AFL-Induced Skin Barrier Injury Mouse Model

To establish a reliable AFL-induced skin injury model, two parameter sets were compared: parameter I (30 W power, 10 ms pulse delay, 0.6 mm fractional spacing) versus parameter II (20 W power, 0.5 ms pulse delay, 0.7 mm fractional spacing). Pathological evaluation on day 7 revealed that areas treated with parameter I exhibited persistent scab formation and epidermal defects, indicating injury beyond intrinsic repair thresholds. In contrast, parameter II achieved complete epidermal restructuring by day 7, demonstrating morphological patterns consistent with clinical AFL-induced skin regeneration (Figure 2A,B). These findings validated parameter II as the optimal AFL protocol for subsequent studies.

Keratinocytes, serving as structural pillars of the epidermal barrier, rely on coordinated interactions between keratin networks and intercellular lipids to maintain integrity. Dynamic phenotypic observations under parameter II revealed dense scab formation within 24 h post-AFL, followed by scab shedding initiating at day 5 and near-complete detachment by day 7, though residual microdamage persisted microscopically (Figure 2C). Histopathological analysis via H&E staining delineated the repair cascade: immediate full-thickness epidermal ablation and superficial dermal thermal damage were observed post-procedure, with re-epithelialization commencing from the basal layer at 24 h. Neo-epidermal coverage was completed by 72 h, epidermal thickness was restored alongside scab exfoliation at day 5, and full wound closure without scarring was achieved by day 7 (Figure 2D). Immunofluorescence staining further demonstrated the reduced expression of differentiation marker K10 and basal marker K14, highlighting AFL-induced thermal interference with keratinocyte protein dynamics and epidermal homeostasis (Figure 2E).

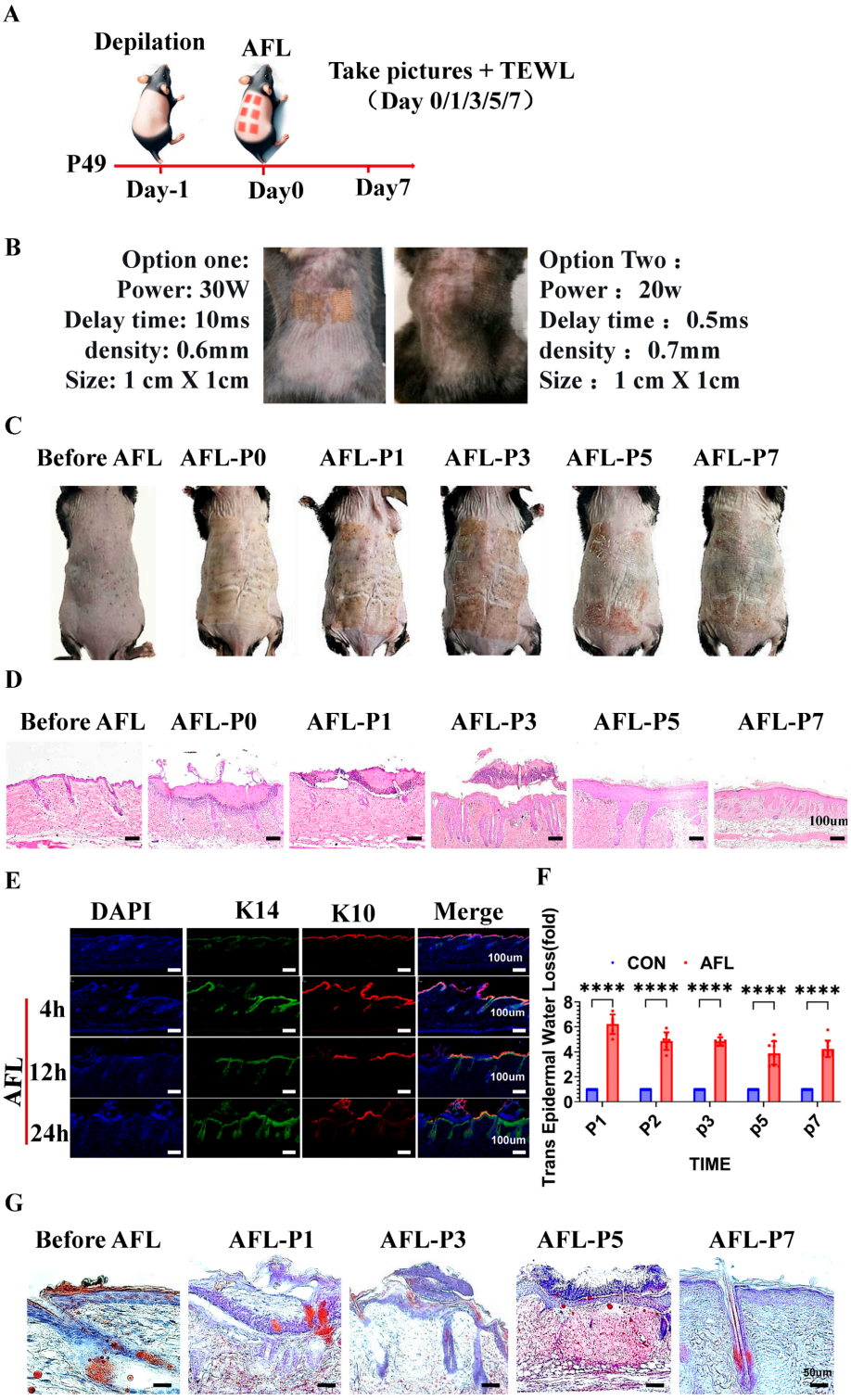


Figure 2. Establishment of an AFL-induced skin barrier injury model and characterization of time-dependent damage. (**A**) Schematic overview of the experimental design for the AFL-induced skin barrier injury model. (**B**) Representative macroscopic images of mouse dorsal skin treated with different AFL parameter settings. (**C**) Phenotypic changes in mouse skin at various time points after AFL treatment. (**D**) H&E staining of skin tissue sections at different time points post-AFL. Scale bar, 100 μm. (**E**) Immunofluorescence staining of epidermal markers (DAPI, K14, and K10) in skin tissue at 4, 12, and 24 h after AFL. Scale bar, 100 μm. (**F**) Quantitative analysis of TEWL in the CON and AFL groups over time. (**G**) Oil Red O staining of skin tissue sections at different time points after AFL. Scale bar, 50 μm. All experiments were performed with at least five biological replicates. Statistical significance: **** $p < 0.0001$.

The integrity of the skin barrier also hinges on stratum corneum lipid metabolism. GPSkin system measurements revealed persistently elevated TEWL, confirming compromised water retention capacity post-AFL (Figure 2F). Oil Red O staining corroborated these findings, showing complete absence of continuous lipid signals in AFL-treated regions compared to the intact lipid distribution in normal skin, thereby confirming AFL-induced spatial disruption of the epidermal lipid layer (Figure 2G). Collectively, these multidimensional analyses establish that parameter II successfully models the dual structural and functional impacts of clinical AFL on the epidermal barrier within controlled damage parameters, providing a robust AFL model for mechanistic investigations.

3.3. SSO Restores Post-AFL Epidermal Barrier via Promoting Lipid Synthesis

To investigate the reparative effects of SSO on AFL-induced epidermal barrier disruption, SSO was daily applied topically to murine dorsal skin post-AFL, with longitudinal monitoring of wound healing phenotypes and TEWL (Figure 3A). The results showed comparable scab shedding patterns between SSO-treated and control groups, with complete scab loss by day 5 and complete re-epithelialization by day 7, indicating that SSO does not affect the natural progression of post-wound epidermal regeneration (Figure 3B). However, TEWL assessments showed that SSO effectively suppressed AFL-induced TEWL elevation as early as 24 h post-injury. The inhibitory effect became more pronounced by 48 h and was sustained through day 7, suggesting that SSO enhances the functional restoration of the epidermal barrier (Figure 3C).

Since improved hydration retention is often linked to stratum corneum lipid metabolism, Oil Red O staining was employed to evaluate lipid deposition. During acute phases (P1, P3, and P5), no significant difference in lipid staining intensity was observed between SSO-treated and control groups, indicating SSO's inability to counteract early-phase lipid metabolic disruption. Strikingly, by day 7, SSO-treated skin exhibited restored lipid deposition at physiological levels, while controls retained widespread lipid-deficient phenotypes (Figure 3D). These results demonstrate that SSO improves epidermal barrier function through, at least in part, the upregulation of lipid biosynthesis pathways. This mechanistic insight positions SSO as a targeted therapeutic candidate for promoting functional barrier restoration following AFL-based dermatological procedures.

3.4. SSO Increases the Expression of PPARα and PPARγ in Epidermis After AFL

PPARs play a pivotal role in regulating cutaneous lipid synthesis and barrier function. The PPAR family comprises three members, namely, PPARα, PPARβ/δ, and PPARγ, which collectively govern lipid metabolism, keratinocyte differentiation, and inflammatory responses, thereby maintaining skin barrier homeostasis. Immunofluorescence staining revealed distinct expression patterns of PPAR isoforms under varying conditions. In normal skin, PPARα maintains constitutive low-level expression, but undergoes upregulation following AFL treatment, Notably, topical application of SSO potentiated this PPARα induction, a response mechanistically aligned with SSO's established role in stimulating cutaneous lipid biosynthesis (Figure 4A,B).

PPARβ/δ displayed minimal expression in normal skin and only modest induction post-AFL, with no additional modulation observed in SSO-treated skin (Figure 4C,D). Notably, PPARγ maintains low basal expression in healthy skin, showing slight elevation after AFL. Strikingly, SSO treatment induced a marked enhancement of PPARγ expression (Figure 4E,F), aligning with its capacity to stimulate lipid synthesis. Complementary RT-PCR analysis of mRNA levels corroborated these immunofluorescence findings, showing that SSO further upregulated the AFL-induced mRNA expression of PPARα and PPARγ, but not PPARβ/δ (Figure 4G–I). These differential responses suggest that SSO preferen-

tially activates PPARα and PPARγ pathways rather than PPARβ/δ after AFL treatment. These findings establish PPARα/γ signaling as the principal potential molecular effector underlying SSO's therapeutic benefits in post-AFL barrier recovery.

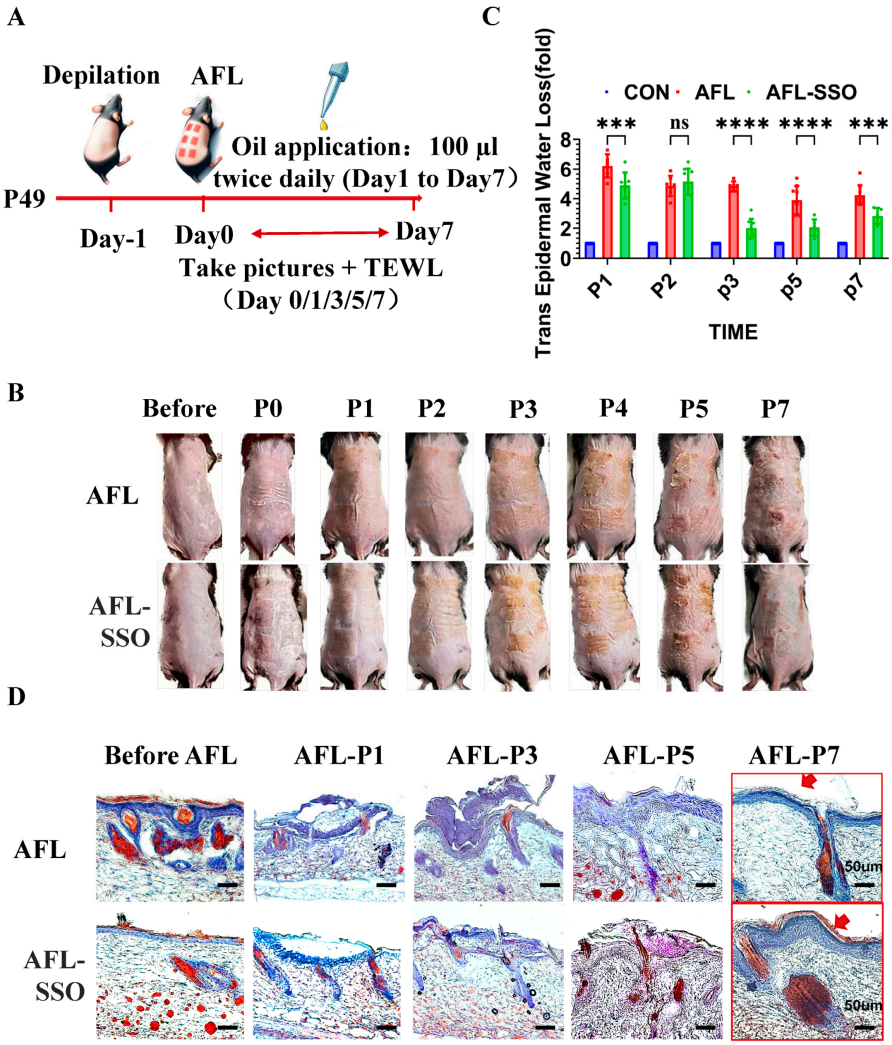


Figure 3. SSO restores post-AFL epidermal barrier via lipid synthesis. (**A**) Schematic overview of the in vivo experimental design for evaluating the therapeutic effect of SSO on AFL-induced skin barrier damage. (**B**) Representative macroscopic images of mouse dorsal skin at different time points after AFL and AFL-SSO treatment. (**C**) Quantitative analysis of TEWL over time in the CON, AFL, and AFL-SSO groups ($n \geq 5$). (**D**) Representative Oil Red O staining of mouse skin sections at different time points following treatment. The red arrows denote whether epidermal lipid formation is present or absent. Scale bar, 50 µm. Statistical significance: ns, not significant ($p > 0.05$); *** $p < 0.001$; **** $p < 0.0001$.

3.5. Inhibition of PPARγ Signaling Attenuates Epidermal Lipid Synthesis After SSO Treatment

To delineate the potential mechanistic targets, we next administrated PPARα inhibitor and PPARγ inhibitor in the skin using intraperitoneal injection and topical administration respectively (Figure 5A). Oil Red O staining on day 7 demonstrated that PPARα inhibition failed to alter SSO-induced lipid accumulation, whereas PPARγ suppression markedly reduced lipid deposition, paralleling the TEWL reversal (Figure 5B,C). TEWL measurements indicated that PPARγ inhibition did not affect the early barrier-protective effects of SSO during the initial 3-day post-wounding period (Figure 5C). However, both systemic and topical PPARγ inhibition markedly reduced the therapeutic efficacy of SSO from day 3 post-injury onward (Figure 5C). Notably, wound closure rates showed no significant differences

among treatment groups, suggesting that PPARγ signaling does not directly influence re-epithelialization processes (Figure 5D). These results imply that SSO may promote barrier recovery, potentially via increased PPARγ expression and subsequent enhancement of epidermal lipid synthesis, thereby supporting the reconstruction of the lamellar lipid layer.

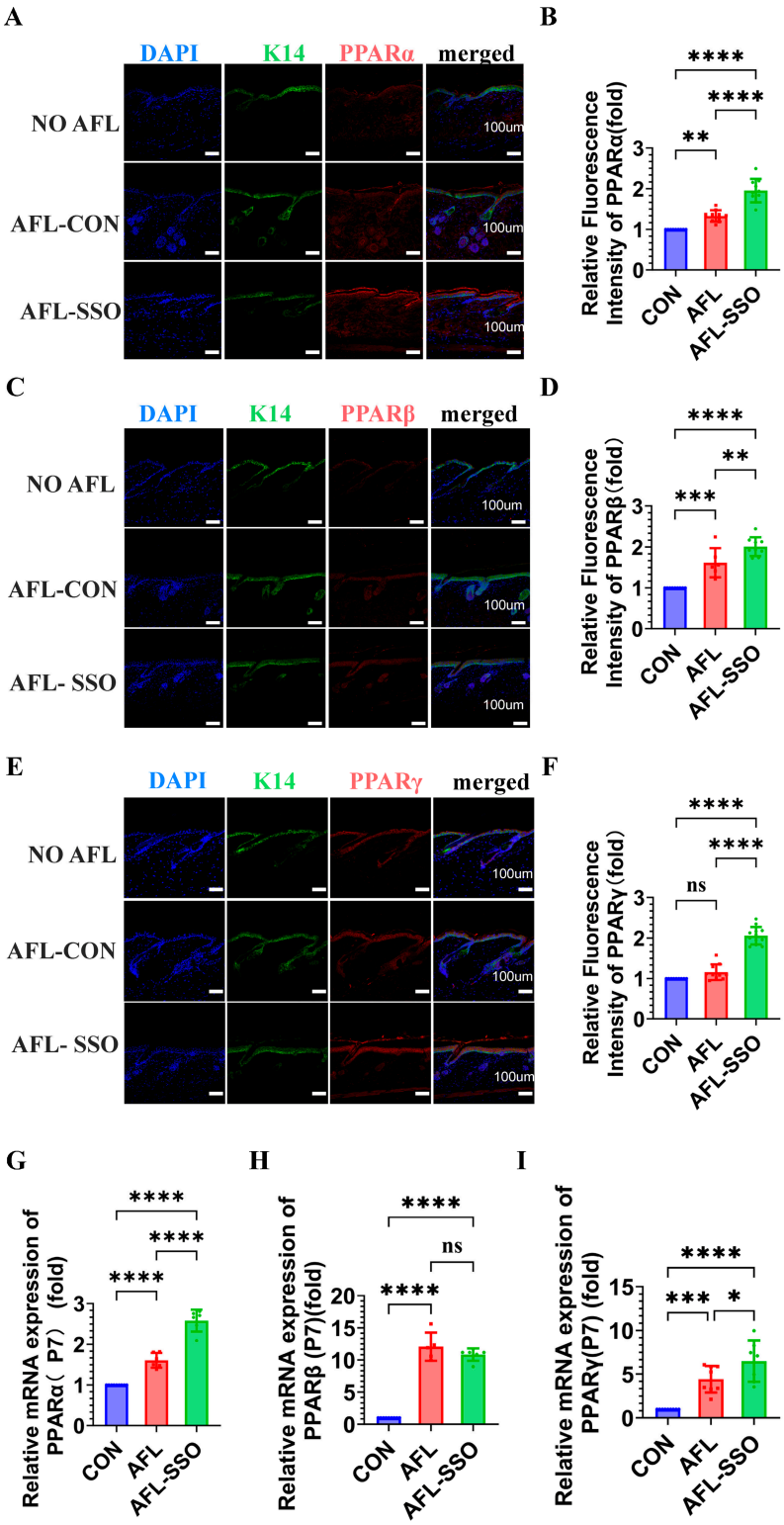


Figure 4. SSO increases epidermal PPAR expression after AFL. (**A**,**B**) Immunofluorescence staining and quantitative analysis of epidermal PPARα expression in the No AFL, AFL, and AFL-SSO groups on day 7. Each red dot in quantitative analysis is a selected field of view from five different mouse

skin tissues, and the relative fluorescence intensity of each field was analyzed with ImageJ. (**C**,**D**) Immunofluorescence staining and quantitative analysis of epidermal PPARβ expression. (**E**,**F**) Immunofluorescence staining and quantitative analysis of epidermal PPARγ expression. Scale bar, 100 μm. (**G–I**) RT-PCR quantification of epidermal PPARα, PPARβ, and PPARγ mRNA levels, respectively. All experiments were performed with at least five biological replicates. Not significant (ns, $p > 0.05$); * $p < 0.05$; ** $p < 0.01$; *** $p < 0.001$; **** $p < 0.0001$.

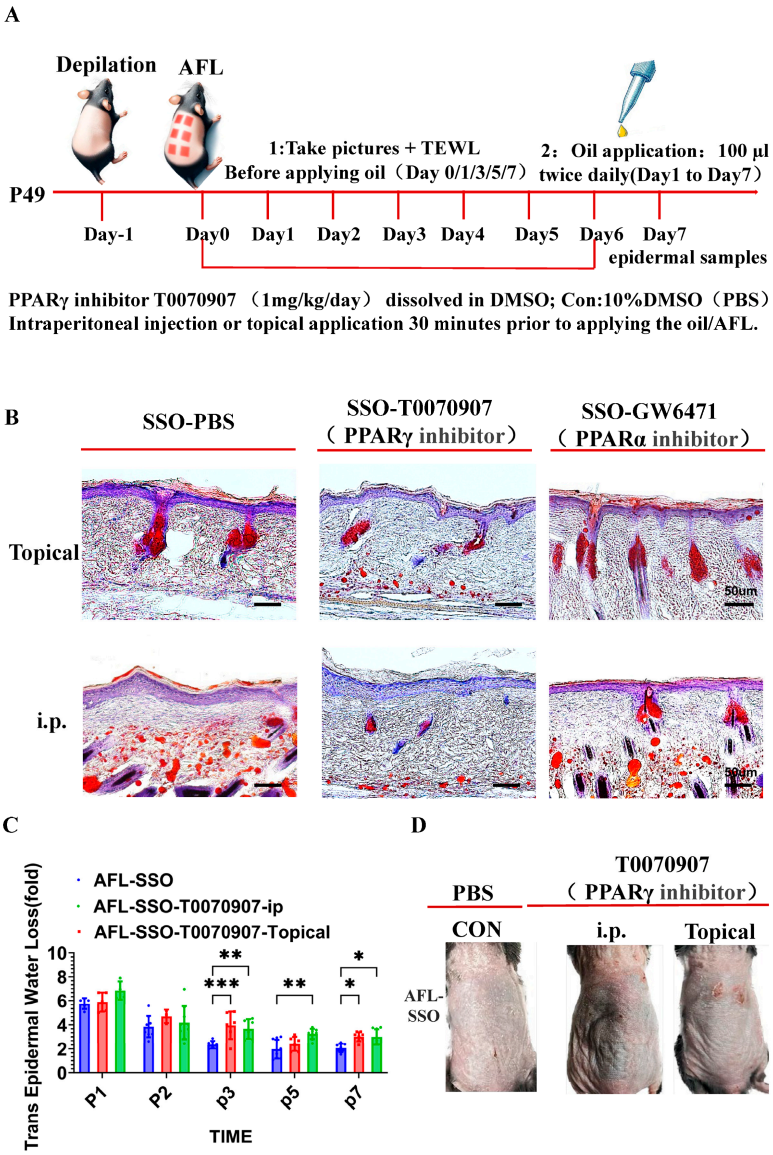


Figure 5. (**A**) Schematic overview of the animal experimental design. (**B**) Representative histological sections of mouse dorsal skin on day 7 after SSO treatment with or without PPARα/γ inhibitors via topical or intraperitoneal administration. Scale bar, 50 μm. (**C**) TEWL changes over time in the AFL-SSO group and groups treated with the PPARγ inhibitor T0070907. (**D**) Representative macroscopic images of mouse dorsal skin on day 7. $n \geq 5$. * $p < 0.05$; ** $p < 0.01$; *** $p < 0.001$.

4. Discussion

This study validated the efficacy of SSO in accelerating epidermal barrier restoration after AFL injury. Chemical characterization confirmed that SSO is a glycerol ester-rich natural oil, with high contents of linoleic acid (69.1%) and oleic acid (18.7%), in addition to abundant vitamin E compounds, polyphenols, and other bioactive constituents, which exhibit potent antioxidant and anti-inflammatory activities, as well as wound-healing and moisturizing effects [36]. Linoleic acid plays a critical role in supporting epidermal lipid

synthesis, promoting ceramide production, and modulating inflammatory responses [37], thereby contributing to skin barrier restoration, relief of dryness, soothing of irritation, and reduction in inflammation [38,39]. The optimized AFL model steadily impaired skin barrier function, characterized by elevated TEWL, disrupted lipid architecture and aberrant keratinocyte differentiation, while retaining endogenous re-epithelialization capability. SSO rapidly normalized barrier function within 24 h and restored epidermal lipid homeostasis on day 7, without affecting wound scab shedding and epidermal regeneration. Mechanistically, AFL injury led to a moderate elevation in cutaneous PPARγ expression, which was further upregulated following SSO treatment. Pharmacological inhibition assays verified that SSO-mediated lipid synthesis and barrier repair were predominantly dependent on the expression of PPARγ. PPARα, γ, and β all play roles in skin lipid formation and metabolism, with PPARγ exhibiting the most prominent effects [17]. Activated PPARγ controls the biosynthesis of neutral lipids and phospholipids and regulates sebocyte function; tissue-specific PPARγ deletion causes sebaceous gland dysplasia and scarring alopecia [40]. In contrast, PPARβ primarily promotes keratinocyte differentiation and inhibits cell proliferation. PPARβ activation inhibits lipid release during sebocyte apoptosis, indicating divergent or even opposing functions of PPAR subtypes in sebum regulation [41]. Consistently, the present study found that PPARβ/δ expression was not elevated following SSO application, suggesting that it may not serve as the core target for SSO-mediated lipid repair. Previous studies have suggested that SSO exerts its effects on reducing TEWL, enhancing hydration, and restoring the skin barrier through linoleic acid-mediated activation of PPARα [21,42,43]. However, our findings indicate that PPARγ plays a predominant role in SSO-mediated epidermal lipid restoration. Interestingly, a recent study on rosacea reported that epidermal lipid metabolism is dysregulated in rosacea patients, with a marked elevation of linoleic acid levels [44]. This elevated linoleic acid was found to hyperactivate PPARγ signaling in the epidermis, thereby suppressing rosacea-like dermatitis, a phenomenon observed in both rosacea patients and mouse models. Based on these findings, we hypothesize that SSO may upregulate PPARγ expression via its linoleic acid component. Increased PPARγ expression would not only promote epidermal lipid synthesis but may also contribute to the mitigation of AFL-induced skin inflammation. Of course, this still requires more detailed follow-up studies for confirmation—for example, directly treating AFL-exposed mouse skin with linoleic acid or oleic acid and examining PPAR expression and lipid synthesis.

Notably, SSO exhibits a biphasic repair pattern in AFL-damaged skin. Functional barrier improvement occurred within 24–48 h, while significant structural lipid reconstruction was only observed on day 7. This temporal dissociation demonstrates that SSO's early barrier protection is independent of lipid biosynthesis regulation. As a natural lipid extract, SSO provides rapid physical protection via surface occlusion and moisturization to reduce acute water loss and external irritation. Meanwhile, its bioactive constituents alleviate acute skin inflammation to attenuate early barrier damage. These early non-lipid protective effects synergize with late lipid metabolism modulation, achieving comprehensive and durable skin barrier repair, and supplement the multi-dimensional mechanism of SSO against AFL-induced skin injury. Overall, SSO promotes barrier restoration by further refining epidermal biological functions on the basis of general wound healing, including improved TEWL and enhanced epidermal lipid synthesis.

Despite the solid in vivo evidence demonstrated in this work, several limitations should be noted for future improvement. First, the specific monomeric components of SSO responsible for PPARγ activation remain unclear, and possible synergistic or antagonistic interactions among different constituents need further exploration. Second, we used only small-molecule inhibitors of PPARγ and PPARα to investigate the mechanism by which

SSO restores lipid synthesis, which is indeed a limitation. Although the PPARγ inhibitor T0070907 is highly selective, with an affinity for PPARγ that is more than 800-fold higher than for PPARα and PPARβ, both intraperitoneal injection and topical application may still result in unpredictable off-target effects and side effects. The most definitive approach would be to use epidermis-specific conditional knockout of PPARγ and PPARα to truly determine whether SSO acts through PPARγ to restore lipid synthesis. Third, Oil Red O staining provides useful qualitative information regarding neutral lipid accumulation, but it does not fully characterize the stratum corneum lipid matrix responsible for barrier function. In future studies, lipidomics analysis should be performed to enable quantitative evaluation of relevant lipid classes, such as ceramides, cholesterol, and free fatty acids, which would provide a more comprehensive understanding of lipid metabolic remodeling. Finally, all experiments were performed on murine models. Given the interspecific differences in skin lipid composition, repair kinetics and inflammatory responses between mice and humans, the clinical translational potential of SSO requires further validation in human keratinocytes or ex vivo human skin models.

In summary, these findings suggest that SSO may contribute to the repair of AFL-induced skin barrier damage, at least in part, through a PPARγ-associated lipid regulatory mechanism. This work adds to the current understanding of natural plant oil-mediated skin protection and may offer a potential reference for clinical adjuvant care following AFL cosmetic procedures.

Supplementary Materials: The following supporting information can be downloaded at: https://www.mdpi.com/article/10.3390/cosmetics13050240/s1, Table S1: Primer list used for RT-PCR; Table S2: RT-PCR reaction system; Table S3: RT-PCR reaction conditions; Table S4: Relative Mass Content of SSO Components; Table S5: Fatty Acid Composition Analysis of SSO (High-Mass Fraction).

Author Contributions: J.L.: Investigation, Validation, Methodology, Formal Analysis, and Writing—Original Draft. Q.W.: Resources and Methodology. J.Z.: Investigation and Methodology. X.W.: Investigation and Methodology. H.J.: Resources and Methodology. Y.W.: Validation and Data Curation. Y.C.: Resources and Methodology. R.L.: Resources and Methodology. G.M.: Writing—Review and Editing, Supervision, Project Administration, Funding Acquisition, and Conceptualization. All authors have read and agreed to the published version of the manuscript.

Funding: This research was funded by the National Natural Science Foundation of China (No. 32570986) and the Natural Science Foundation of Shanghai (No. 23ZR1431900).

Institutional Review Board Statement: All experimental procedures were conducted in compliance with the ARRIVE guidelines and approved by the Institutional Animal Care and Use Committee (IACUC) of Shanghai Jiao Tong University (Approval Code 202401045, Approval Date 21 February 2024), with strict adherence to the 3Rs principles (Replacement, Reduction, Refinement).

Data Availability Statement: The data presented in this study are available on request from the corresponding authors.

Conflicts of Interest: Qian Wang, HaidongJia, Yuanyuan Chen, and Runshuang Lu are employed by Shanghai Jahwa United Co., Ltd. The sponsor had no role in the design of the present study; in the analysis or interpretation of data; in the writing of the manuscript; or in the decision to publish the results. All authors that the research was conducted in the absence of any commercial or financial relationships that could be construed as a potential conflict of interest.

References

1. Belokhvostova, D.; Berzanskyte, I.; Cujba, A.-M.; Jowett, G.; Marshall, L.; Prueller, J.; Watt, F.M. Homeostasis, regeneration and tumour formation in the mammalian epidermis. *Int. J. Dev. Biol.* **2018**, *62*, 571–582. [CrossRef]
2. McLafferty, E.; Hendry, C.; Alistair, F. The integumentary system: Anatomy, physiology and function of skin. *Nurs. Stand.* **2012**, *27*, 35–42. [CrossRef]

3. Zhang, Y.; Wen, D.; Ho, C.; Liu, Y.; Wang, X.; Zhou, Z.; Gao, Y.; Li, Q. HDAC5 deacetylates cytosolic ACTN4 during skin reepithelialization and represents a therapeutic target for chronic wound healing. *Sci. Transl. Med.* **2025**, *17*, eads0594. [CrossRef]
4. Di, R.; Du, Q.; Xie, Y.; Lu, Y.; Gao, W.; Zhang, L.; Qi, X.; Fan, Y.; Li, J.; Wang, F.; et al. A mechano-resistance mechanism in skin adapts to terrestrial locomotion. *Cell* **2025**, *188*, 5797–5808.e16. [CrossRef]
5. Leprince, C.; Simon, M. Epidermal lamellar bodies, essential organelles for the skin barrier. *Front. Cell Dev. Biol.* **2025**, *13*, 1597884. [CrossRef]
6. Feingold, K.R.; Elias, P.M. Role of lipids in the formation and maintenance of the cutaneous permeability barrier. *Biochim. Biophys. Acta (BBA)-Mol. Cell Biol. Lipids* **2014**, *1841*, 280–294. [CrossRef]
7. Bouwstra, J.A.; Nădăban, A.; Bras, W.; McCabe, C.; Bunge, A.; Gooris, G.S. The skin barrier: An extraordinary interface with an exceptional lipid organization. *Prog. Lipid Res.* **2023**, *92*, 101252. [CrossRef]
8. Liu, B.; Yang, L.; Yang, H.; Wang, L.; Liang, K.; Wang, Q.; Yang, R. A biomimetic multifunctional dressing based on stratum corneum microstructure: Integrating antibacterial barrier and breathability for enhanced wound healing. *Biomaterials* **2026**, *326*, 123639. [CrossRef]
9. Murata, T.; Honda, T.; Mostafa, A.; Kabashima, K. Stratum corneum as polymer sheet: Concept and cornification processes. *Trends Mol. Med.* **2022**, *28*, 350–359. [CrossRef]
10. Tierney, E.P.; Hanke, C.W.; Petersen, J. Ablative fractionated CO_2 laser treatment of photoaging: A clinical and histologic study. *Dermatol. Surg.* **2012**, *38*, 1777–1789. [CrossRef]
11. Guo, H.; Zhang, X.; Li, H.; Fu, C.; Jiang, L.; Hu, Y.; Huang, J.; Chen, J.; Zeng, Q. Dynamic panoramic presentation of skin function after fractional CO2 laser treatment. *iScience* **2023**, *26*, 107559. [CrossRef]
12. Yoshida, K.; Yokouchi, M.; Nagao, K.; Ishii, K.; Amagai, M.; Kubo, A. Functional tight junction barrier localizes in the second layer of the stratum granulosum of human epidermis. *J. Dermatol. Sci.* **2013**, *71*, 89–99. [CrossRef]
13. Bencini, P.L.; Guida, S. Skin Resurfacing: Ablative and Non-ablative Lasers. In *Technology in Practical Dermatology: Non-Invasive Imaging, Lasers and Ulcer Management*; Fimiani, M., Rubegni, P., Cinotti, E., Eds.; Springer International Publishing: Cham, Switzerland, 2020; pp. 357–367.
14. Christensen, R.L.; Son, H.G.; Zhou, E.Y.; Olesen, U.H.; Garibyan, L.; Farinelli, W.A.; Sakamoto, F.H.; Rox Anderson, R.; Haedersdal, M.; Demehri, S. Cutaneous Immune Responses to Ablative Fractional Laser, Heat- and Cold-Based Dermatological Procedures. *Lasers Surg. Med.* **2025**, *57*, 101–111. [CrossRef]
15. Rawlings, A.V.; Schoop, R.; Klose, C.; Monneuse, J.-M.; Summers, B.; Voegeli, R. Changes in levels of omega-O-acylceramides and related processing enzymes of sun-exposed and sun-protected facial stratum corneum in differently pigmented ethnic groups. *Int. J. Cosmet. Sci.* **2022**, *44*, 166–176. [CrossRef]
16. Li, Y.-Y.; Ye, L.-R.; Cui, Y.-Z.; Xu, F.; Chen, X.-B.; Zhang, F.-F.; Lu, Y.; Zheng, Y.-X.; Man, X.-Y. DGAT2 reduction and lipid dysregulation drive psoriasis development in keratinocyte-specific SPRY1-deficient mice. *JCI Insight* **2025**, *10*, e192507. [CrossRef]
17. Zhu, B.; Zhu, X.; Borland, M.G.; Ralph, D.H.; Chiaro, C.R.; Krausz, K.W.; Ntambi, J.M.; Glick, A.B.; Patterson, A.D.; Perdew, G.H.; et al. Activation of Peroxisome Proliferator-Activated Receptor-β/δ (PPARβ/δ) in Keratinocytes by Endogenous Fatty Acids. *Biomolecules* **2024**, *14*, 606. [CrossRef]
18. Maeng, J.; Jeong, S.; Kim, H.; Nam, G. Multi-Target Strategies for Enhancing Ceramide Production: A Review of Bioactive Ingredients in Cosmetic Science. *Cosmetics* **2026**, *13*, 8. [CrossRef]
19. Bhardwaj, V.; Pal, A.; Goel, F. ABCA12 and stress: A molecular insight into lipid transport and cellular resilience. *Psychopharmacology* **2026**, *243*, 683–693. [CrossRef]
20. Kumar, A.P.; Puthussery, D.T. Regulation of PPAR-γ coactivator-1α and its implication in mitochondrial function and neurodegenerative diseases. *Ageing Res. Rev.* **2025**, *112*, 102887. [CrossRef]
21. Vaughn, A.R.; Clark, A.K.; Sivamani, R.K.; Shi, V.Y. Natural oils for skin-barrier repair: Ancient compounds now backed by modern science. *Am. J. Clin. Dermatol.* **2018**, *19*, 103–117. [CrossRef]
22. Chon, S.-H.; Tannahill, R.; Yao, X.; Southall, M.D.; Pappas, A. Keratinocyte differentiation and upregulation of ceramide synthesis induced by an oat lipid extract via the activation of PPAR pathways. *Exp. Dermatol.* **2015**, *24*, 290–295. [CrossRef]
23. Somjorn, P.; Kamanamool, N.; Kanokrungsee, S.; Rojhirunsakool, S.; Udompataikul, M. A cream containing linoleic acid, 5% dexpanthenol and ceramide in the treatment of atopic dermatitis. *Asian Pac. J. Allergy Immunol.* **2024**, *42*, 361–367. [CrossRef]
24. Takeda, S.; Shimoda, H.; Takarada, T.; Imokawa, G. Strawberry seed extract and its major component, tiliroside, promote ceramide synthesis in the stratum corneum of human epidermal equivalents. *PLoS ONE* **2018**, *13*, e0205061. [CrossRef]
25. Furue, K.; Mitoma, C.; Tsuji, G.; Furue, M. Protective role of peroxisome proliferator-activated receptor α agonists in skin barrier and inflammation. *Immunobiology* **2018**, *223*, 327–330. [CrossRef]
26. Kim, S.O.; Han, Y.; Ahn, S.; An, S.; Shin, J.C.; Choi, H.; Kim, H.-J.; Park, N.H.; Kim, Y.-J.; Jin, S.H.; et al. Kojyl cinnamate esters are peroxisome proliferator-activated receptor α/γ dual agonists. *Bioorganic Med. Chem.* **2018**, *26*, 5654–5663. [CrossRef]
27. Majewski, G.; Craw, J.; Falla, T. Accelerated Barrier Repair in Human Skin Explants Induced with a Plant-Derived PPAR-α Activating Complex via Cooperative Interactions. *Clin. Cosmet. Investig. Dermatol.* **2021**, *14*, 1271–1293. [CrossRef]

28. Akiyama, M. The roles of ABCA12 in keratinocyte differentiation and lipid barrier formation in the epidermis. *Dermatoendocrinol* **2011**, *3*, 107–112. [CrossRef]
29. Tachibana, K.; Fukuda, S.; Fukushima, J.; Ishimoto, K.; Sakata, M.; Nishimori, Y.; Doi, T. Exploring compounds to be used as cosmetic agents that activate peroxisome proliferator-activated receptor alpha. *Int. J. Cosmet. Sci.* **2022**, *44*, 189–200. [CrossRef]
30. Song, L.; Geng, S.; Liu, B. Characterization of Wei Safflower Seed Oil Using Cold-Pressing and Solvent Extraction. *Foods* **2023**, *12*, 3228. [CrossRef]
31. *ISO 16128-2:2017*; Cosmetics—Guidelines on Technical Definitions and Criteria for Natural and Organic Cosmetic Ingredients—Part 2: Criteria for Ingredients and Products. ISO: Geneva, Switzerland, 2017.
32. Bouallegue, K.; Allaf, T.; Besombes, C.; Younes, R.B.; Allaf, K. Phenomenological modeling and intensification of texturing/grinding-assisted solvent oil extraction: Case of date seeds (*Phoenix dactylifera* L.). *Arab. J. Chem.* **2019**, *12*, 2398–2410. [CrossRef]
33. Liu, J.; Wang, Q.; Zhong, J.; Wang, X.; Zhang, M.; Wang, Y.; Zhao, Y.; Zhu, L.; Lu, R.; Jia, H.; et al. Safflower Seed Oil and Fermented *Artemisia annua* Oil Restore UVB-Induced Skin Barrier Dysfunction by Attenuating Inflammation and Promoting Extracellular Matrix Remodeling. *Cosmetics* **2026**, *13*, 77. [CrossRef]
34. Morin, S.; Simard, M.; Rioux, G.; Julien, P.; Pouliot, R. Alpha-Linolenic Acid Modulates T Cell Incorporation in a 3D Tissue-Engineered Psoriatic Skin Model. *Cells* **2022**, *11*, 1513. [CrossRef]
35. Simard, M.; Tremblay, A.; Morin, S.; Martin, C.; Julien, P.; Fradette, J.; Flamand, N.; Pouliot, R. α-Linolenic acid and linoleic acid modulate the lipidome and the skin barrier of a tissue-engineered skin model. *Acta Biomater.* **2022**, *140*, 261–274. [CrossRef]
36. Adeleke, B.S.; Babalola, O.O. Oilseed crop sunflower (*Helianthus annuus*) as a source of food: Nutritional and health benefits. *Food Sci. Nutr.* **2020**, *8*, 4666–4684. [CrossRef]
37. Wang, X.; Jia, Y.; He, H. The role of linoleic acid in skin and hair health: A review. *Int. J. Mol. Sci.* **2024**, *26*, 246. [CrossRef]
38. Yamunadevi, P.; Michelle, S. Sunflower seeds (*Helianthus annuus*) and health benefits: A review. *Recent Prog. Nutr.* **2023**, *3*, 1–5. [CrossRef]
39. Karagounis, T.K.; Gittler, J.K.; Rotemberg, V.; Morel, K.D. Use of "natural" oils for moisturization: Review of olive, coconut, and sunflower seed oil. *Pediatr. Dermatol.* **2018**, *36*, 9–15. [CrossRef]
40. Liu, Y.; Ji, S.; Gao, H.; Chen, H.; Xiang, J.; Cui, S.; Zouboulis, C.C.; Cai, A.; Fu, X.; Sun, X. Sebaceous gland reprogramming with a single gene, PPARG, and small molecules. *Signal Transduct. Target. Ther.* **2023**, *8*, 286. [CrossRef]
41. Schuster, M.; Zouboulis, C.C.; Ochsendorf, F.; Müller, J.; Thaci, D.; Bernd, A.; Kaufmann, R.; Kippenberger, S. Peroxisome proliferator-activated receptor activators protect sebocytes from apoptosis: A new treatment modality for acne? *Br. J. Dermatol.* **2011**, *164*, 182–186. [CrossRef]
42. Yang, M.; Zhou, M.; Song, L. A review of fatty acids influencing skin condition. *J. Cosmet. Dermatol.* **2020**, *19*, 3199–3204. [CrossRef]
43. Pratami, R.R.E.; Budiastuti, A.; Riyanto, P.; Malik, D.A.; Widayati, R.I.; Muslimin; Hardian. Sunflower seed oil for skin barrier repair in newborns: A systematic review and meta-analysis with biophysical parameters. *J. Pak. Assoc. Dermatol.* **2022**, *32*, 85–95.
44. Wang, M.; Xiao, W.; Liu, T.; Zhu, Y.; Chen, M.; Tan, Z.; Xu, S.; Zhao, Z.; Liu, F.; Xie, H.; et al. Linoleic acid improves rosacea through repairing mitochondrial damage in keratinocytes. *Life Med.* **2025**, *4*, lnaf005. [CrossRef]

Disclaimer/Publisher's Note: The statements, opinions and data contained in all publications are solely those of the individual author(s) and contributor(s) and not of MDPI and/or the editor(s). MDPI and/or the editor(s) disclaim responsibility for any injury to people or property resulting from any ideas, methods, instructions or products referred to in the content.